Bulletin of the Chemical Society of Japan

Ultrahigh-CO_2 Adsorption Capacity and CO_2/N_2 Selectivity by Nitrogen-Doped Porous Activated Carbon Monolith

Akram A. Alabadi,* Haider A. Abbood, Ammar S. Dawood, and Bien Tan

Advance Publication on the web January 21, 2020
doi:10.1246/bcsj.20190336

Ultrahigh-CO_2 Adsorption Capacity and CO_2/N_2 Selectivity by Nitrogen-Doped Porous Activated Carbon Monolith

Akram A. Alabadi[*1,2], Haider A. Abbood[3] , Ammar S. Dawood[3] and Bien Tan[2]

[1]South Refineries Company, Ministry of Oil, Basra, 61006, Iraq.

[2]School of Chemistry and Chemical Engineering, Huazhong University of Science and Technology, Luoyu Road No. 1037, Wuhan, 430074, China.

[3]Material Engineering Department, College of Engineering, University of Basrah, Basarah, 61006, Iraq.

E-mail: akram.aladdae@gmail.com

Akram Alabadi
Akram Alabadi received PH.D. Degree from Huazhong University of Science &Technology in 2014.
I have worked as chemist in South Refineries Company (SRC) in Basrah, Iraq since Bch. Graduated at 2001 until now.

Abstract

Among microporous adsorbents, N- doped activated carbon monolith has been actual developed to achieve functionalized nanoporous carbon via cross-linked polymer precursors, which are used Friedel-craft alkylation and pyrolysis. Nitrogen-doping establish to be an efficient method for boosting the CO_2 adsorption capacity of carbon-based adsorbents, research in this area is still full of challenges to reach a fit doping level of nitrogen (N) and intrinsic microporosity. Herein, an easy method is that enables the preparation of microporous nitrogen-doped porous carbon monolith with proportion of 4.6 wt% N, which employs poly (H-BINAM) as primary material. By virtue of chemical activation, large microporosity is generated and gives build to a monolithic structured porous nitrogen-doped activated carbon (MPC-700). The results showed a remarkable CO_2 adsorption capacity (6.74 mmol g^{-1} at 273 K and 5.18 mmol g^{-1} at 298 K under 1 bar), and an excellent CO_2 over N_2 selectivity (153), which is measured from the single-component adsorption isotherms according to Henry's Law. This value overrides the CO_2 over N_2 selectivity of thus reported for carbon-based adsorbents contain on a diverse nitrogen doped ones, which features are largely associated with the remarkably high N-content furthermore the partial graphitic framework.

Keywords: CO_2 adsorption, activated carbon, monolith, microporous material.

1. Introduction

Hierarchical N-doped porous carbons (HPCs) monolithic with a continuous three dimensional (3D) framework have received broad attentions and research during the recent decades due to their potentially technological application as sorbents for toxic gas separation and greenhouse gas capture for their well-defined pore dimensions and morphology.[1-4] Synthetic polymer established hierarchical nanostructured carbons are great attractive for their consistent pore dimensions which can be adaptable on long length scales, For this reason, diffusibility of guest species could be improved through its distinctive hierarchical pores.[5, 6] N-doped HPC monolith is nowadays considered one of the most viable ways to exhibit multifaceted features such as tunable textural properties, excellent thermal and chemical stability, which are noteworthy physicochemical properties that are responsible of micro/nanostructured porous carbons perfect candidates for emerging substrates in nanotechnology science.[7-9]

Environmental issues, such as Climate change caused by the emissions of greenhouse gases, among which Anthropogenic CO_2 contributes more than 60%, is one of the most serious threats mankind.[10-12] To tackle this problem, Current attempts towards the optimization of materials in terms of CO_2 uptake/selectivity, wherefore in recent years, a large amount of efforts has been diverted to the design and construction of hierarchically structured porous materials of nanoscale pores and topologies, for example, monolithic materials as sorbents with high performance for CO_2 capture and storage.[13-15] Several solid adsorbents such as metal organic frameworks (MOF), zeolites, coordination organic polymers (COPs), activated carbons (ACs) and amine containing porous materials have been studied for CO_2 capture.[16-23] Among those mostly study porous materials, activated carbons are one of them, which have received due attention for their different uses, for instances, as battery electrodes, as super capacitors [24, 25] or gases sorbents.[26, 27] ACs are particularly ideal alternative adsorbents for their ease of synthesis, low cost, composite structure, tunable textural properties, excellent CO_2 adsorption, high selectivity and stability and ease of regeneration.[28-30]

The research investigating multiple benefits of (i.e. N, S, B, P) doping into carbon matrix of physicochemical properties is one of surge, leading to the improved performance in manifold uses such as electrochemical capacitance for super capacitors[16, 31-34], heterogeneous catalysis,[19, 35] oxygen reduction for fuel cells [36] and gas adsorption and selectivity.[11, 37] Meanwhile, the search of both nano-architectural design and surface modification of order porous carbon monolith by doping is hot in the present material science field.[13, 38] It is noteworthy, that nitrogen-doped or amine-supported porous materials are selective towards CO_2 over N_2, due to the strong acid-base interaction between the amines and CO_2,[13, 26] and their capacity for CO_2 capture are much less influenced by the presence of moisture compared with sorbents that depend on physisorption only.[39-41] As has been reported previously, N-doped porous carbon materials prepared from lignocelluloses show an excellent performance for CO_2 capture with 4 mmole g^{-1} at 298 K and 1 atm,[36] while N-doped carbon produced by the chemical

activation of polypyrrole have a CO_2 capacity of 4.5 mmol g^{-1} at 298 K and 1 atm and good CO_2/N_2 selectivity (approximately 124:1)[6] and amidoxime-modified porous carbon shows a CO_2 capacity of 4.97 mmol g^{-1} at 273 K and 1 atm, and enhanced CO_2/N_2 selectivity.[42]

This study, therefore reports the experiment on nitrogen-containing monolith porous carbons (MPC-700) with a developed pore structure using a new hyper cross-linked polyamine (H-BINAM) as carbon and nitrogen source, in which KOH is adopted as activation agents to promote micropore formation during activation, with carbons of high CO_2 uptake of ca. 2.3 mmol g^{-1} at 0.15 bar, 298K and high CO_2/N_2 selectivity up to 153 (calculated by initial slope method), in the attempt to provide further experimental evidence on the importance of narrow micropores and nitrogen doping for high CO_2 uptake under ambient conditions.

2. Experimental

2.1 Synthesis of H-BINAM and MPC-700

Hyper cross-linked polymer (H-BINAM) reaction was conducted in a three-necked flask (150 mL) equipped with a stirring bar and a water-cooled reflux. Preparation of H-BINAM was made through Friedel-Crafts reaction. In a typical reaction, 20 mL of 1,2-Dichloroethylene (DCE) and 1.80 g of anhydrous aluminum trichloride ($AlCl_3$) was placed into the flask, which was then placed into a water bath of 80°C, the right temperature for the reaction, when the solution was vigorously stirred at room temperature before later, 0.60 g of [1,1'-Binaphthalene]-2,2'-diamine (BINAM) was added into the solution 20 hours later after the reaction, the obtained white product was filtered, and purified using Soxhlet extraction with methanol for 24 h., and the obtained solid product was dried at 70 °C for overnight (yield 83%). The hyper cross-linked polymer obtained was named H-BINAM.

Carbonization of H-BINAM was performed by placing a crucible boat with a mixture of as-prepared H-BINAM (1 g) and dry KOH (4 g) in a tube furnace under the flowing nitrogen .The carbonization temperature was raised simultaneously to 700 °C and then was held at 700 °C for 2 h under the nitrogen flow. Monolithic porous carbon were formed and naturally cooled to room temperature. Then, the obtained black monolithic porous carbon were then completely washed three times with HCl solution (10 wt%) to remove any remaining inorganic salts and thereafter washed thoroughly with deionized water until a neutral pH was measured. Finally, the activated carbon monolith was dried in an oven at 65 °C in vacuum oven overnight. This final product obtained was donated as MPC-700.

2.2 Characterization of materials

The morphology, microstructure and composition of H-BINAM and MPC-700 samples were examined by field emission scanning electron microscopy (FE-SEM, SIRION 200, EI, Nederland) at 5 kV, high resolution transmission electron microscopy (HRTEM, TECNAI G2 20) electron microscope operated at 200 kV. Fourier-transform infrared (FTIR) spectroscopy of polymer and N-AC samples were carried out by Bruker Vertex 70 spectrometer (Germany). The solid state ^{13}C cross-polarization magic angle spinning (CP/MAS) NMR spectra were obtained on a WB 400 MHz Bruker Advance II spectrometer equipped with a 4 mm double-resonance MAS probe and a spinning frequency of 10 kHz. X-ray photoelectron spectrometer (XPS -AXIS-ULTRA DLD high- performance imaging, Shimadzu, Japan) were used to analyze the functional groups on surface and the chemical composition of samples.

Nitrogen sorption/adsorption isotherms and textural properties were measured at 77 K using nitrogen with a conventional volumetric technique by a Micrometrics ASAP 2020 volumetric sorptometer. Prior to measurement, the samples were degassed under vacuum at 200 °C for ca. 12 h until the pressure was less than 5 mmHg .The surface area (S_{BET}) was determined by the conventional BET (Brunauer–Emmett–Teller) . The pore size distribution was calculated by NL-DFT method with a slit pore model built from the nitrogen adsorption data.

3. Results and Discussion

3.1 Morphology of sample

The procedure for the synthesis of H-BINAM and MPC-700 is shown in Figure 1. The microporous carbon is synthesized by a two-step procedure. In the first step, crosslinked polymer precursors are prepared *via Friedel-Crafts* reaction in the presence of $AlCl_3$ as a catalyst. Nitrogen doped monolithic porous carbon (MPC-700) are synthesized through the pyrolysis with a chemical agent (KOH) of hyper cross-linked polymer (H-BINAM) as carbon precursor.

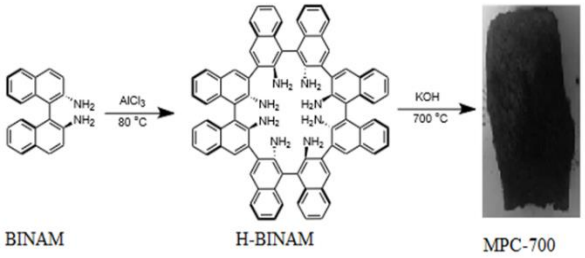

Figure 1. Schematic illustration of fabrication route of H-BINAM and its conversion to functional monolith porous carbon (MPC-700).

The FTIR spectra of H-BINAM and MPC-700 are compared in Figure 2. For H-BINAM, the band observed at 3430 cm^{-1} is due to N-H stretching. In the meantime, the NH_2– stretching vibrations of the secondary amine (C–N) are assigned at 1132, and 773 cm^{-1}.[26] The absorption bands at 2921-2780 cm^{-1} are attributed to asymmetric and symmetric C-H stretching vibrations, and the absorption peak shown at 1652-1630 cm^{-1} is attributed to C=C stretching in aromatic rings.[43, 44] The bands obtained at 1600-1500 cm^{-1} corresponds to C-H stretching in aromatic compounds. In addition, there are no FTIR bands in accordance with the imine linkage stretching vibration around 1610 cm^{-1}. After the chemical activation and pyrolysis, FTIR structures of the MPC-700, and the peaks intensity are reduced.

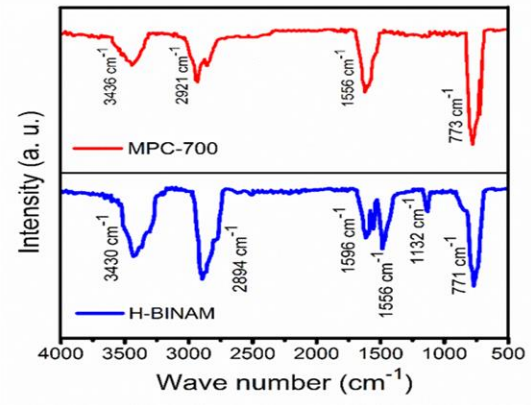

Figure 2. FT-IR spectra of the H-BINAM and MPC-700 samples.

H-BINAM is also characterized at the molecular level by solid state ^{13}C cross-polarization magic-angle spinning (CP/MAS) NMR spectroscopy, the spectra and the assignment of the resonances are shown in Figure 3. Specifically, the signal at ~142 ppm corresponds to the phenyl carbons bonded with the nitrogen atom (N-Car). The signal at ~131 ppm can be attributed to other substituted phenyl carbon atoms (Car–H). Finally, the signals at ~124 ppm is due to the unsubstituted phenyl carbons (Car–Car).[43] Additionally, the peak at 38 ppm indicates the methylene carbon formed by the Friedel Crafts alkylation reaction.

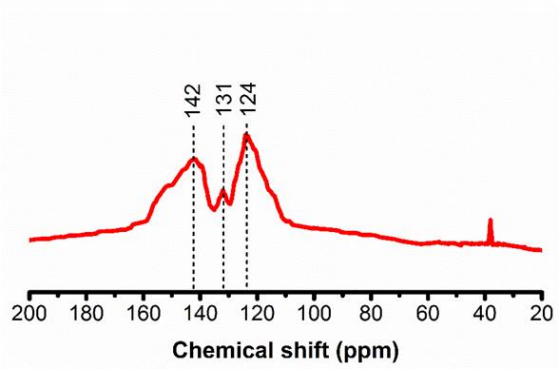

Figure 3. Solid-state ^{13}C CP/MAS NMR spectra of H-BINAM.

H-BINAM and MPC-700 are observed under scanning electron microscopy (FE-SEM) and transmission electron microscopy (HRTEM) techniques and their results are shown in Figure 4. FE-SEM images demonstrate that the H-BINAM surface is smooth and compact without any clear pores, while the MPC-700 is morphologically monolithic with irregular shape, which exhibits highly interconnected pores. The important fact is that the morphology of MPC-700 changes much after carbonization process with KOH, showing a porous framework with large mesopores and abundant macropores as shown in Figure **4** (A-B). HRTEM measurements are also carried out to further study the microstructures of the as-synthesized MPC-700 material. It can be seen from Figure **4** (C–D), that there is a structurally defective porous structure with a local aromatic ordering and highly interconnected pores and channels in the nano-scaled range, with a highly porous network morphology.

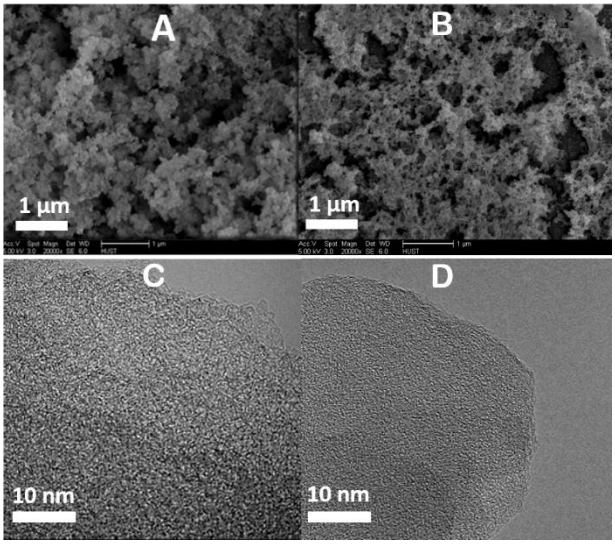

Figure 4. FE-SEM and HRTEM images of HPNAM (A&C) and MPC-700 (B&D).

The nitrogen sorption isotherms (77K) and the corresponding PSD plots for the as-synthesis polymer and monolithic activated carbons show Type I isotherms with high gas uptake at low pressures according to the (IUPAC) classification, with an obvious small hysteresis loop especially in H-BINAM isotherm, suggesting the existence of the mesoporous structure (Figure 5a). The S_{BET} surface area of the H-BINAM is a notable 776 $m^2 g^{-1}$. Due to the activation, MPC-700 exhibits an increase with S_{BET} to1930 $m^2 g^{-1}$. Additionally, the pore volume increased from 0.65 to 1.45 $cm^3 g^{-1}$, while the pore size from 2.19 to 1.72 nm. These data indicate that activating agents develop an additional porosity, especially microporosity, in the carbon studied. The adsorption capacity of the activated carbons increase with the shift of adsorption isotherms. The pore size distribution (PSD) pattern (Figure 5b) and the quantitative results (Table 1) provide further verification.

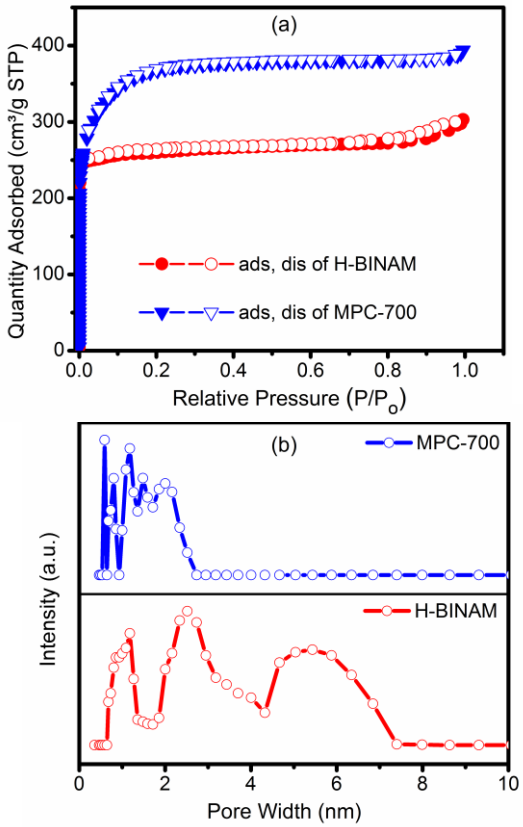

Figure 5. Nitrogen sorption isotherms measured at -196 °C (a) and pore size distributions (b) of H-BINAM and MPC-700 samples, analyzed on N_2 adsorption isotherms measured at 77 K using the NLDFT model.

Table 1. Porous texture properties and CO_2 uptakes of samples.

Sample	BET Surface Area ($m^2 g^{-1}$)	Pore Volume ($cm^3 g^{-1}$)	Dominant Pore Size (nm)	CO_2 uptake at >1bar (mmol g^{-1})	
				273K	298K
H-BINAM	776	0.65	2.19	5.81	4.12
MPC-700	1930	1.45	1.72	6.74	5.18

XPS technique was employed to investigate the number and type of the nitrogen functional groups existed on the surface of the sorbents. The XPS N1s spectra of illustrative N-doped sample MPC-700 is shown in Figure 6, three main peaks related to the MPC-700 were observed at 398.5, 399.9 and 401.3 eV. These peaks can be appointed to pyridinic-N (N-6), pyrrolic-N (N-5) and quaternary-N (N-Q), respectively.[45] Quantitative analysis illustrates that expect for MPC-700, the amount of various nitrogen species are 4.6 wt % in the order of N-5>N-6>N-Q for this activated carbon.[21]

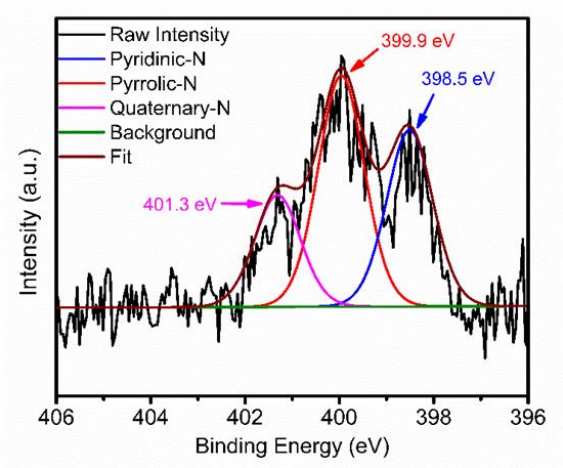

Figure 6. N 1s XPS spectra of the MPC-700 sample.

3.2 CO_2 adsorption

The microporous nature, the high surface area and the functionalization of these H-BINAM and MPC-700 promoted us to investigate their gas adsorption properties. The CO_2 adsorption capacity of both H-BINAM and MPC-700 are measured up to 1 bar at 273 K and 298 K on a Micromeritics ASAP 2020 static volumetric analyzer. Statistics and experimental results have shown that the CO_2 uptakes in nanoporous materials depend not only on the specific surface area or pore volume, but also on functional groups, pore sizes, and other variability at the molecular level. The corresponding CO_2 adsorption isotherms and uptakes are plotted and summarized in Figure 7 and Table 1, respectively MPC-700 exhibits the highest CO_2 uptake of 6.74 and 5.18 mmole.g^{-1} at 273 K and 298 K respectively at 1.13 bar, while H-BINAM shows the highest CO_2 uptake of 5.82 and 4.12 mmole.g^{-1} at 273 K and 298 K respectively. This adsorption capacity is one of the best values mentioned for carbonaceous materials. [5, 46-48]

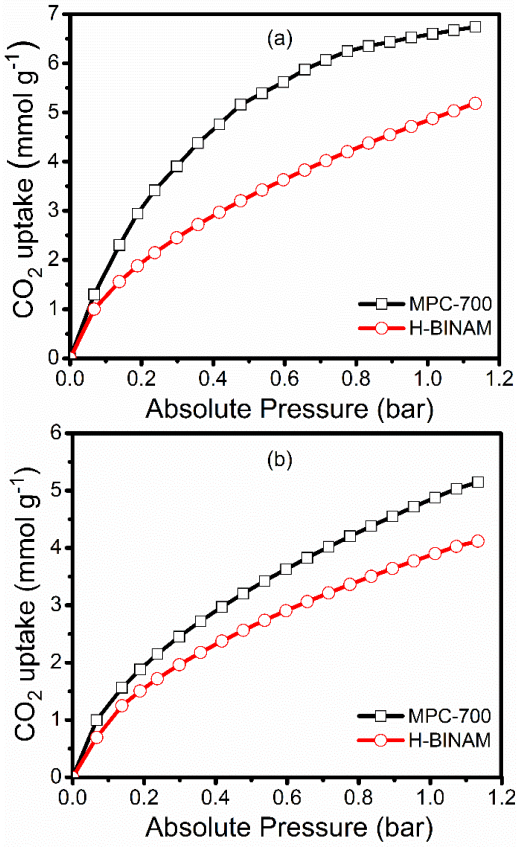

Fig. 7 CO_2-adsorption performance of H-BINAM and MPC-700 samples at 273K (a) and 298K (b).

3.3 Selectivity

High selectivity of the N- doped activated carbon is an excellent indicator of the materials performance in separating CO_2 from the gas mixtures. To increase CO_2/N_2 selectivity one way is to raise basicity of the carbon material, which will improve the CO_2 uptake via acid-base interaction.[49] Therefore, to evaluate CO_2/N_2 selectivity, nitrogen adsorptions on H-BINAM and MPC-700 are investigated under 273K and 298 K (Figure 8). Although H-BINAM only display a moderate CO_2 capacity possible due to their low surface area compared to MPC-700, both samples exhibit remarkable CO_2/N_2 adsorption selectivity. Selectivity of CO_2/N_2 is measured using Henry's Law through the initial slopes of CO_2 and N_2 adsorption isotherms.[50] From the initial slopes of N_2 and CO_2 adsorption isotherms, the final results CO_2/N_2 selectivity of H-BINAM and MPC-700 are 102 and 153 respectively, comparable to or better than those obtained with reported nitrogen-doped carbons, which proves that nitrogen doping and high surface area are more preferential to the enhancement of CO_2/N_2 selectivity.[51-53]

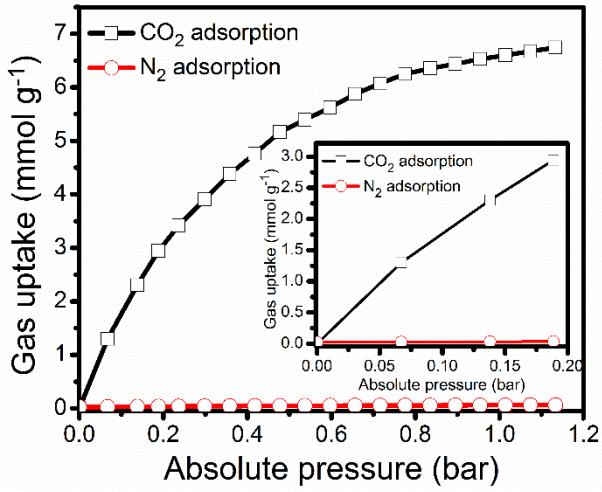

Figure 8. Gas adsorption performance of H-BINAM and MPC-700: CO_2 and N_2 at 273 K.

3.4 Heat of adsorption (Qst).

The isosteric heats of adsorption (Qst) for representative N-decorated carbons are measured from the CO_2 sorption isotherms determined at 273 K and 298 K using the Clausius−Clapeyron equation as shown in Figure 9. The Qst values at the initial adsorption stage are 43.1 kJ mol^{-1} for MPC-700 and 33.5 kJ mol^{-1} for H-BINAM, which is higher than and similar to the Qst values for typical carbon adsorbents with amine-functionalized materials reported previously. MPC-700 has higher Qst under low coverage range compared with the hypercross-linked polymer H-BINAM. The higher Qst in the initial phase leads to a distinctive adsorption of CO_2 and therefore the selectivity to N_2, which may be attributed to the huge amounts of narrow micropores and tuneable nitrogen content in MPC-700. As well as, the improved interaction between the adsorbent and CO_2 molecules, an excessive elevation of Qst (e.g. in the cases of chemisorption) would lead to be obstacle in sorbent regeneration.[18]

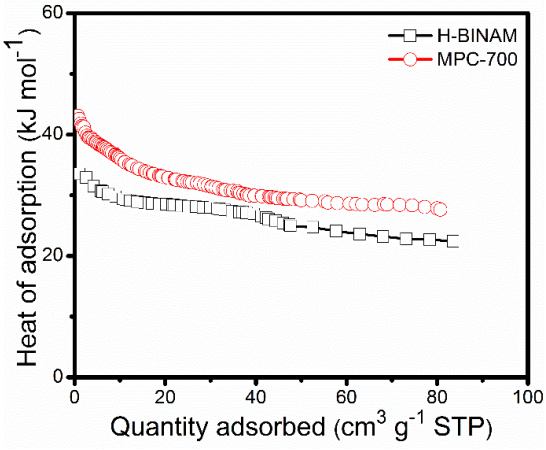

Figure 9. Isosteric heat of adsorption calculated by the dual-site Langmuir isotherm fits at 273 and 298 K.

4. Conclusion

A new type of monolith carbonaceous adsorbents with a high CO_2 adsorption capacity was prepared from hyper cross-linked polymer (H-BINAM). The doped N was found to be present in pyridine (N-6), pyrrolic/pyridone (N-5) and quaternary (N-Q) nitrogen compounds with graphite-like structure. The N-doped activated carbon monolithic in this work were demonstrated to have a great potential in greenhouse-gas capture and clean energy applications.The uptake capacity for CO_2 is up to 6.74 mmol g^{-1} and 5.18 mmol g^{-1} (1 bar and 273 K and 298 K respectively). Moreover, the good selectivity of the MPC-700 toward CO_2 over N_2 it has a promising potential application in gas separation.

Acknowledgement

The authors thank the Analytical and Testing Center of Huazhong University of Science & Technology for their assistance in characterization of the samples. This work was supported by the South Refineries Company (SRC) & the National Natural Science Foundation of China (No. 50973037, 51173058), the Program for New Century Excellent Talents in University from the Ministry of Education of China (No. NCET-10-0389), and the Hubei Province Natural Science Fund for Distinguished Young Scholars (No.2011CDA109).

References

1 S. Dutta, A. Bhaumik, K. C. W. Wu, *Energy Environ. Sci.* **2014**, *7*, 3574-3592 10.1039/c4ee01075b.

2 C. Zhang, R. Kong, X. Wang, Y. Xu, F. Wang, W. Ren, Y. Wang, F. Su, J.-X. Jiang, *Carbon* **2017**, *114*, 608-618 10.1016/j.carbon.2016.12.064.

3 L. Xia, X. Li, Y. Wu, M. Rong, *ACS Sustainable Chemistry & Engineering* **2015**, *3*, 1724-1731 10.1021/acssuschemeng.5b00243.

4 C. Chen, H. Huang, Y. Yu, J. Shi, C. He, R. Albilali, H. Pan, *Chemical Engineering Journal* **2018**, *353*, 584-594 10.1016/j.cej.2018.07.161.

5 M. Yang, L. Guo, G. Hu, X. Hu, J. Chen, S. Shen, W. Dai, M. Fan, *Industrial & Engineering Chemistry Research* **2016**, *55*, 757-765 10.1021/acs.iecr.5b04038.

6 J. W. To, J. He, J. Mei, R. Haghpanah, Z. Chen, T. Kurosawa, S. Chen, W. G. Bae, L. Pan, J. B. Tok, J. Wilcox, Z. Bao, *J Am Chem Soc* **2016**, *138*, 1001-9 10.1021/jacs.5b11955.

7 A. Beltzung, A. Klaue, C. Colombo, H. Wu, G. Storti, M. Morbidelli, *Energy Technol.* **2018**, *6*, 718-727 10.1002/ente.201700649.

8 W. Sangchoom, R. Mokaya, *ACS Sustainable Chemistry & Engineering* **2015**, *3*, 1658-1667 10.1021/acssuschemeng.5b00351.

9 J. Wang, R. Ma, Y. Zhou, Q. Liu, *J. Mater. Chem. A* **2015**, *3*, 12836-12844 10.1039/c5ta01679g.

10 J. Huang, X. Zhou, A. Lamprou, F. Maya, F. Svec, S. R. Turner, *Chemistry of Materials* **2015**, *27*, 7388-7394 10.1021/acs.chemmater.5b03114.

11 M. Peyravi, *Polymers for Advanced Technologies* **2018**, *29*, 319-328 10.1002/pat.4117.

12 L. Yue, L. Rao, L. Wang, L. An, C. Hou, C. Ma, H. DaCosta, X. Hu, *Energy & Fuels* **2018**, *32*, 6955-6963 10.1021/acs.energyfuels.8b01028.

13 Lalit A. Darunte, Yuri Terada, Christopher R. Murdock, Krista S. Walton, David S. Sholl, a. C. W. Jones, *ACS Applied Materials & Interfaces* **2017**, *9* 17042-17050.

14 D. Qian, C. Lei, E. M. Wang, W. C. Li, A. H. Lu, *ChemSusChem* **2014**, *7*, 291-8 10.1002/cssc.201300585.

15 P. Zhang, Y. Zhong, J. Ding, J. Wang, M. Xu, Q. Deng, Z. Zeng, S. Deng, *Chemical Engineering Journal* **2019**, *355*, 963-973 10.1016/j.cej.2018.08.219.

16 D. H. Jo, H. Jung, S. Jeon, S. H. Kim, *Bulletin of the Chemical Society of Japan* **2016**, *89*, 1462-1469 10.1246/bcsj.20160286.

17 D. Andirova, C. F. Cogswell, Y. Lei, S. Choi, *Microporous and Mesoporous Materials* **2016**, *219*, 276-305 10.1016/j.micromeso.2015.07.029.

18 J. Zhu, P. M. Usov, W. Xu, P. J. Celis-Salazar, S. Lin, M. C. Kessinger, C. Landaverde-Alvarado, M. Cai, A. M. May, C. Slebodnick, D. Zhu, S. D. Senanayake, A. J. Morris, *J Am*

Chem Soc **2018**, *140*, 993-1003 10.1021/jacs.7b10643.

19 X. Su, L. Bromberg, V. Martis, F. Simeon, A. Huq, T. A. Hatton, *ACS Appl Mater Interfaces* **2017**, *9*, 11299-11306 10.1021/acsami.7b02471.

20 G. Srinivas, V. Krungleviciute, Z.-X. Guo, T. Yildirim, *Energy Environ. Sci.* **2014**, *7*, 335-342 10.1039/c3ee42918k.

21 Z. Wang, H. Ren, S. Zhang, F. Zhang, J. Jin, *ChemSusChem* **2018**, *11*, 916-923 10.1002/cssc.201702243.

22 H. Zhang, W. Tian, Z. Qian, T. Ouyang, M. Saunders, J. Qin, S. Wang, M. O. Tadé, H. Sun, *Carbon* **2018**, *133*, 306-315 10.1016/j.carbon.2018.03.044.

23 L. Keller, B. Ohs, L. Abduly, M. Wessling, *Chemical Engineering Journal* **2019**, *359*, 476-484 10.1016/j.cej.2018.11.100.

24 Z. Li, K. Guo, X. Chen, *RSC Advances* **2017**, *7*, 30521-30532 10.1039/c7ra02701j.

25 Y. Kado, K. Imoto, Y. Soneda, N. Yoshizawa, *Journal of Power Sources* **2016**, *305*, 128-133 10.1016/j.jpowsour.2015.11.093.

26 L. Yue, Q. Xia, L. Wang, L. Wang, H. DaCosta, J. Yang, X. Hu, *J Colloid Interface Sci* **2018**, *511*, 259-267 10.1016/j.jcis.2017.09.040.

27 Y. Zhang, Y. Chi, C. Zhao, Y. Liu, Y. Zhao, L. Jiang, Y. Song, *Journal of Chemical & Engineering Data* **2017**, *63*, 202-207 10.1021/acs.jced.7b00824.

28 X. Li, L. Zhu, Q. Xue, X. Chang, C. Ling, W. Xing, *ACS Appl Mater Interfaces* **2017**, *9*, 31161-31169 10.1021/acsami.7b09648.

29 X. He, K. Mei, R. Dao, J. Cai, W. Lin, X. Kong, C. Wang, *AIChE Journal* **2017**, *63*, 3008-3015 10.1002/aic.15647.

30 A. Alabadi, H. A. Abbood, Q. Li, N. Jing, B. Tan, *Sci Rep* **2016**, *6*, 38614 10.1038/srep38614.

31 P. Fu, L. Zhou, L. Sun, B. Huang, Y. Yuan, *RSC Advances* **2017**, *7*, 13383-13389 10.1039/c7ra00433h.

32 A. Alabadi, S. Razzaque, Z. Dong, W. Wang, B. Tan, *Journal of Power Sources* **2016**, *306*, 241-247 10.1016/j.jpowsour.2015.12.028.

33 Y. Sun, K. Li, J. Zhao, J. Wang, N. Tang, D. Zhang, T. Guan, Z. Jin, *J Colloid Interface Sci* **2018**, *526*, 174-183 10.1016/j.jcis.2018.04.101.

34 J.-G. Lu, X. Li, Y.-X. Zhao, H.-L. Ma, L.-F. Wang, X.-Y. Wang, Y.-F. Yu, T.-Y. Shen, H. Xu, Y.-T. Zhang, *Environmental Chemistry Letters* **2018**, *17*, 1031-1038 10.1007/s10311-018-00822-4.

35 S. Xu, K. Song, T. Li, B. Tan, *J. Mater. Chem. A* **2015**, *3*, 1272-1278 10.1039/c4ta05265j.

36 B. Zhu, K. Qiu, C. Shang, Z. Guo, *J. Mater. Chem. A* **2015**, *3*, 5212-5222 10.1039/c4ta06072e.

37 J. Zhou, Z. Li, W. Xing, T. Zhu, H. Shen, S. Zhuo, *Chem Commun (Camb)* **2015**, *51*, 4591-4 10.1039/c4cc10364e.

38 N. Balahmar, A. S. Al-Jumialy, R. Mokaya, *Journal of Materials Chemistry A* **2017**, *5*, 12330-12339 10.1039/c7ta01722g.

39 J. Wang, R. Krishna, X. Wu, Y. Sun, S. Deng, *Langmuir* **2015**, *31*, 9845-52 10.1021/acs.langmuir.5b02390.

40 J. Wang, R. Krishna, J. Yang, S. Deng, *Environ Sci Technol* **2015**, *49*, 9364-73 10.1021/acs.est.5b01652.

41 C. Chen, Y. Yu, C. He, L. Wang, H. Huang, R. Albilali, J. Cheng, Z. Hao, *Applied Surface Science* **2018**, *439*, 113-121 10.1016/j.apsusc.2017.12.217.

42 S. M. Mahurin, J. Górka, K. M. Nelson, R. T. Mayes, S. Dai, *Carbon* **2014**, *67*, 457-464 10.1016/j.carbon.2013.10.018.

43 X. Wang, Y. Zhao, L. Wei, C. Zhang, J.-X. Jiang, *J. Mater. Chem. A* **2015**, *3*, 21185-21193 10.1039/c5ta05230k.

44 K. Tian, Z. Wu, F. Xie, W. Hu, L. Li, *Energy & Fuels* **2017**, *31*, 12477-12486 10.1021/acs.energyfuels.7b02223.

45 H. S. Kim, M. S. Kang, S. Lee, Y.-W. Lee, W. C. Yoo, *Microporous and Mesoporous Materials* **2018**, *272*, 92-100 10.1016/j.micromeso.2018.06.021.

46 J. Choma, M. Marszewski, L. Osuchowski, J. Jagiello, A. Dziura, M. Jaroniec, *ACS Sustainable Chemistry & Engineering* **2015**, *3*, 733-742 10.1021/acssuschemeng.5b00036.

47 F. Akhtar, N. Keshavarzi, D. Shakarova, O. Cheung, N. Hedin, L. Bergström, *RSC Adv.* **2014**, *4*, 55877-55883 10.1039/c4ra05009f.

48 L. Largitte, T. Brudey, T. Tant, P. C. Dumesnil, P. Lodewyckx, *Microporous and Mesoporous Materials* **2016**, *219*, 265-275 10.1016/j.micromeso.2015.07.005.

49 N. von der Assen, L. J. Muller, A. Steingrube, P. Voll,

A. Bardow, *Environ Sci Technol* **2016**, *50*, 1093-101 10.1021/acs.est.5b03474.

50 Y. Yuan, H. Huang, L. Chen, Y. Chen, *Macromolecules* **2017**, *50*, 4993-5003 10.1021/acs.macromol.7b00971.

51 L. Rao, R. Ma, S. Liu, L. Wang, Z. Wu, J. Yang, X. Hu, *Chemical Engineering Journal* **2019**, *362*, 794-801 10.1016/j.cej.2019.01.093.

52 L. An, S. Liu, L. Wang, J. Wu, Z. Wu, C. Ma, Q. Yu, X. Hu, *Industrial & Engineering Chemistry Research* **2019**, *58*, 3349-3358 10.1021/acs.iecr.8b06122.

53 L. Yue, L. Rao, L. Wang, Y. Sun, Z. Wu, H. DaCosta, X. Hu, *Energy & Fuels* **2018**, *32*, 2081-2088 10.1021/acs.energyfuels.7b03646.